Materials Advances

ROYAL SOCIETY OF CHEMISTRY

PAPER

View Article Online
View Journal

Cite this: DOI: 10.1039/d6ma00413j

Dissolved oil and mercury(II) adsorption under dynamic conditions by thiol-terminated COF-modified sponges

Panagiota Bika, [a] Nadia Todorova, [a] Theopisti Lymperopoulou, [b] Lamprini-Areti Tsakanika, [b] Maria-Anna Gatou, [b] Elias Sakellis, [ac] Nikolaos Zacharopoulos, [a] Vassilis Psycharis, [a] Apostolos Kalafatis, [a] Thomas Stergiopoulos, [a] Dimitrios Tsoukleris, [d] Evangelia A. Pavlatou [b] and Panagiotis Dallas *[ae]

In this work, a multi-step approach for the fabrication of a unique sponge-based platform with multiple functionalities and applications in water-remediation technologies under dynamic conditions is presented. Commercial melamine sponges were rendered hydrophobic through decoration with vinyl-terminated silane and subsequently functionalized *in situ* through a two-step process with a thiol-terminated covalent organic framework (COF). The materials were extensively characterized and applied for the removal of dissolved oil from emulsions and mercury cations under dynamic conditions, namely in a batch reactor under constant stirring for oil adsorption and in a flow reactor with constant metal concentration for Hg adsorption. The chemical and structural stability of the COF networks were evaluated *via* FTIR, EDS, and SEM analysis, respectively. An oil-removal study was conducted using a 100 ppm solution with a volume of 100 mL, was evaluated through UV-vis measurements and the results demonstrated a first-order kinetics fitted with the Elovich model, which provided the initial rate α = 0.307 mg cm^{-3} min^{-1} and desorption constant β = 0.323 g cm^{-3} for the active sites of the thiol-terminated sponges. The competitiveness of a series of elements against mercury adsorption was examined through dynamic absorption experiments and inductively coupled plasma optical emission spectrometry (ICP–OES). Mercury removal efficiencies of 96–99% were achieved over 300 minutes of continuous flow of a 10 ppm solution, while 77–96% removal was achieved over a subsequent 90 minutes for a 100 ppm mercury solution. The characterization analysis and the environmental remediation studies between the efficiencies of COF-modified sponges without and with the –SH terminal groups revealed the crucial role of the thiol pendant groups in the removal of both dissolved oil and mercury. The versatility of the functional material enables its dual functionality in heavily polluted aqueous environments.

Received 25th March 2026,
Accepted 8th April 2026

DOI: 10.1039/d6ma00413j

rsc.li/materials-advances

1. Introduction

The contamination of the aqueous environment with crude oil and heavy metals is an ever-increasing threat due to the lack of effective safety measures in industrial sites and cargo ships.[1,2] Various materials have been proposed for the remediation of aqueous environments and melamine sponges appear as a compelling and versatile platform for such applications.[3] Specifically, sponges have been rendered superhydrophobic for ultra-efficient oil–water separation[4] while their functionalization with COFs and hydrophilic layers[5] has enabled the improvement of oil–water separation/purification.[6,7] Crude oil spills clearly present massive environmental destruction; however, oil-in-water emulsions appear as an even greater danger.[8] Groundwater contamination is a significant health threat for the local population, and even residential areas have been exposed to petroleum hydrocarbon pollution.[9]

[a] *Institute of Nanoscience and Nanotechnology, NCSR Demokritos, 15341, Athens, Greece. E-mail: pdallas@eie.gr, p.dallas@inn.demokritos.gr; Tel: +302107273812*
[b] *Laboratory of General Chemistry, School of Chemical Engineering, National Technical University of Athens, Zografou Campus, 15772, Athens, Greece*
[c] *Department of Physics, National and Kapodistrian University of Athens, Athens, Greece*
[d] *NanoViis Innovative Nanotechnologies 21 El. Venizelou Str., Melissia, 15127, Athens, Greece*
[e] *Theoretical and Physical Chemistry Institute, National Hellenic Research Foundation, 11635, Athens, Greece*

Increased industrialization is also leading to pollution of aqueous resources with heavy metals such as mercury, lead, copper and zinc. Mercury is one of the most toxic heavy metals, with strict regulations for maximum contaminant levels in both water and soil. Soil can be heavily contaminated with mercury due to industrial activities, with concentrations ranging from less than 1 mg kg^{-1} (background levels) up to approximately 10 000 mg kg^{-1} in some cases.[10] Modified sponges are well established as candidates for the removal of heavy metal ions (Hg^{2+}, Pb^{2+}, As^{3+}, and Cd^{2+}) from water.[11] Sponges that were functionalized with biogenic methionine resins have reduced the mercury levels to 1.8–4.4 ppb from 200–400 ppb in only 15 minutes as was outlined in the work by Ali *et al.*[12] A super-amphiphilic silicon sponge was reported to adsorb a high amount of mercury cations with concentrations at the level of 63–6231 ppm. The efficiency of the sponge is related to its porosity and the strong affinity between mercury and sulfur.[13] Furthermore, a polyurethane sponge modified with reduced graphene oxide was suggested for both oil–water separation and the removal of divalent copper from wastewater.[14] This nanocomposite exhibited an ~100% removal within 2 h at a divalent copper concentration of 6 ppm. Finally, magnetic nanoparticles embedded in melamine sponges have effectively adsorbed Pb^{2+} and Cr^{6+} through electrostatic mechanisms.[15]

Recently, we demonstrated the ultra-efficient removal of copper cations from water using a melamine sponge decorated with a triazine-based covalent organic framework (COF) bearing terminal 4,4′-bipyridine units.[16] This work was based on our previous identification of the reaction mechanism and coordination in divalent copper absorbed by COFs in their powder form.[17] However, these COFs suffer from small porosity, as evidenced by BET measurements. To this end, imine-linked COFs appear as optimum systems for heavy metal removal. This subclass of covalent organic frameworks has found applications in gas storage and separation, environmental remediation and catalysis.[18–20] Their organic pendant groups can be further modified with a terminal thiol that presents extraordinary ability for mercury and lead removal.[21] Furthermore, by incorporating vinyl silane groups, the sponges were endowed with superhydrophobic properties, and they have been presented as an ideal system for crude oil removal,[22] substantially changing the initial wetting properties and behavior of the commercial melamine sponges.[23]

In this work, we present a facile synthesis of an imine-based COF functionalized on hydrophobic sponges for ultra-efficient removal of heavy metals and oil from water. The *in situ* reaction is easily scalable with a straightforward modification of more than two (2) grams of melamine sponges in a single batch. The materials absorb crude oil dissolved in water and demonstrate an extraordinary capacity for selective mercury sorption. The former is evidenced by UV-visible spectroscopy and the latter by ICP–OES. The crucial role of the terminal thiol groups in endowing the materials with amphiphilic properties for both oil and heavy metal remediation is investigated. The complete removal of mercury cations and dissolved oil in a short period of time was explained using a first-order kinetic model of oil removal and an accurate fitting with the Elovich equation.

2. Experimental section

2.1. Materials

The commercial Wevora WR-009 melamine sponge was employed as a substrate. Tetraethylorthosilicate (98%, $Si(OC_2H_5)_4$, TEOS) was purchased from Acros and absolute ethanol (99.8%) from Thermo Fisher. Ammonia solution (25%, NH_4OH) was purchased from Carlo Erba, while triethoxyvinylsilane (97%, $C_8H_{18}O_3Si$, VTES) was bought from Thermo Scientific. 1,3,5-Tris(4-aminophenyl) benzene (TAB) 97+% and 2,5-divinylterephthaldehyde (Dva) were purchased from BLDpharm. Tetrahydrofuran and *o*-dichlorobenzene were purchased from Sigma Aldrich and the radical initiator dibenzoyl peroxide, 97% (dry wt), wet with 25% water, from Thermo Scientific Chemicals.

2.2. Synthesis of hydrophobic sponges (Sp_h)

The commercial melamine sponges were rendered hydrophobic after a two-step process. Initially, a silica layer was formed after the condensation of tetraethyl orthosilicate, and then, a second condensation of vinyltrimethoxysilane took place. The synthesis was accomplished following a previously published procedure.[24] The sample is denoted as Sp_h.

2.3. Coating with an imine covalent organic framework (Sp_h_COF)

In a scale-up procedure, the precursors, along with the hydrophobic sponge, reacted *in situ*,[4,8] without the use of a radical initiator. 728 mg of hydrophobic sponge Sp-h is added to 70 mL of *o*-dichlorobenzene and 70 mL of isopropanol. Then, 1.176 g of TAB (3.346 mmol) is added under a continuous argon flow, and the mixture is stirred for 5 minutes at 50 °C, prior to the quick injection of 0.945 g Dva (5.075 mmol) and 10 mL of acetic acid in the dispersion. The flask is heated under reflux and argon flow at 100 °C for 4 hours. Then, the modified sponges are collected *via* filtration, washed with isopropanol and dried under air. The obtained sample is denoted as Sp_h_COF. As a control experiment, the same COF was synthesized by the reaction of TAB with Dva[21] in the absence of the sponge substrates, and the sample is denoted as Powder_ctrl. A second control experiment was performed where a scaled-down condensation reaction in the presence of melamine sponge was left to proceed for 24 hours in toluene (sample denoted as Sp_ctrl).

2.4. Functionalization with 1,2-ethanedithiol (Sp_h_COF_SH)

The weight of the Sp_h_COF was measured at 545 mg, and the modified sponges were dispersed in 52 mL of tetrahydrofuran under argon flow. Then, 2.5 mL of 1,2-ethanedithiol and 52 mg of benzoyl peroxide were added to the suspension. The flask was heated at reflux temperature under argon flow. The final sponges were filtered, washed with isopropanol and acetone,

and dried under air. The obtained sample is denoted as Sp_h_COF_SH.

2.5. Oil-in-water emulsion adsorption

Initially, a concentrated 1000 mg L^{-1} (ppm) emulsion was prepared by adding an appropriate amount of crude oil to 500 mL of deionized water. The crude oil was slowly added (within 10 min) to the water under mixing, and the system was treated for 40 min at a velocity of 5000 rpm using a high shear emulsifier. Then, 50 mL of the prepared emulsion was diluted with deionized water to 500 mL, and the system was treated for 40 min under the same conditions. Thus, a homogeneous oil-in-water emulsion with a concentration of 100 ppm was obtained, which was used for the evaluation of the activity of sponges in diluted oil removal. Then, the sponges were added to the emulsion under constant stirring at room temperature. Aliquots were taken at specific time intervals in order their UV-vis spectra to be measured. Three cycles of adsorption with a duration of 350 min each were performed. After each cycle, the sponges were washed with acetone and air-dried. Samples are denoted as Sp_COF_nc and Sp_COF_SH_nc, where n = 1, 2, 3 represents the number of oil adsorption cycles.

2.6. Heavy metal absorption

Dynamic adsorption experiments were carried out using an experimental setup of two small-scale columns to examine the absorption capacity of the materials. The prepared columns were connected to a two-channel microflow variable-speed peristaltic pump, enabling the simultaneous upward inlet of two solutions into the columns. A single element solution prepared from the $Hg(NO_3)_2$ salt and a multielement solution prepared with appropriate dilution of the 100 mg L^{-1} stock CRM 0D7B (CPA Chem) and then addition of Hg at a concentration of 10 ppm, were injected through the columns with an upward flow of 0.35 mL min^{-1} at ambient temperature. The efficiency is calculated using the relationship $(C_0 - C_t)/C_0$. The effluents, collected from the top of the columns, were stored at 4 °C prior to analysis by inductively coupled plasma optical emission spectrometry (ICP–OES) using an external calibration method.

3. Characterization techniques

The surface morphologies and energy dispersive X-ray spectroscopy (EDS) elemental analysis were examined using scanning electron microscopy (SEM) with a JEOL 7401f field emission microscope. The crystalline structure was analyzed using the X-ray diffraction (XRD) patterns obtained with a Smart Lab Rigaku Diffractometer (Cu Ka radiation). The FTIR spectra were recorded on a Thermo Nicolet iS50 instrument in attenuated total reflection mode from 400 to 4000 cm^{-1}. The diffuse reflectance spectra and the spectra used for the evaluation of oil absorbance were recorded on an Analytik Jena Specord 210 Plus equipped with an integrating sphere. The mercury uptake was studied using an Optima 7000 DV PerkinElmer inductively coupled plasma optical emission spectrometer (ICP–OES). The surface wettability was evaluated through an Ossila contact angle goniometer. The crude oil emulsion was prepared using a high shear emulsifier Silverson L5M-a.

4. Results and discussion

4.1. Chemical and structural characterization of the materials

In this work, hydrophobic melamine sponges were utilized as platforms for the functionalization of an imine-based covalent organic framework.[21] The melamine sponges were initially rendered hydrophobic, through a procedure that involves two subsequent steps of hydrolysis–condensation of the silicon alkoxides TEOS and VTES. The specific reactions for their transformation to silica networks under acidic and alkaline (in our experiment) conditions is well documented in the literature. The mechanism includes (i) gradual hydrolysis of the ethoxy (–OEt) to hydroxyl (–OH) groups and (ii) condensation of H_2O and C_2H_5OH molecules, resulting in the formation of Si–O–Si bonds.[25,26] After this modification, the imine COF was efficiently coated onto the sponges following a modified experimental procedure,[4,8] using hydrophobic sponges as platforms, with the system precursors and Hac as a catalyst. A post-functionalization procedure with 1,2-ethanedithiol resulted in the decoration of the COF with terminal thiol groups, and it was used as the final material for the oil and metal sorption study. The COFs were synthesized with the already established Schiff base condensation reaction between 1,3,5-tris(4-aminophenyl) benzene (Tab) and 2,5-divinylterephthaldehyde (Dva).[27] The final step was performed by employing the well-known thiol–ene coupling reaction, using benzoyl peroxide as an environmentally friendly radical initiator, instead of azobisisobutyronitrile (AIBN). The steps leading to the fabrication of the final orange-brown composite are presented in Fig. 1a. To demonstrate the importance of this system in real-life applications, we focused on synthesizing gram-scale quantities of the materials, and we also summarized the other functional materials that use sponges as a matrix for water remediation in Table 1.

X-ray diffraction was initially employed to prove the formation of a covalent organic framework on the surface of sponges. The two distinctive structures of the COF, before and after the thiol–ene coupling reaction are presented in Fig. 2a. To obtain a direct comparison with the imine COF, we performed the polycondensation reaction in the absence of sponges, which yielded the pristine powder (Powder_ctrl) and additionally a scaled-down reaction was performed employing a heating time of 24 hours in toluene (sample: Sp_ctrl). The XRD patterns of Sp_h_COF and Sp_h_COF_SH are presented in Fig. 2b, alongside the diffraction patterns of the control samples and to obtain a direct comparison with the imine COF powder (Powder_ctrl) and sponge (Sp_ctrl). The functionalized sponge Sp_h_COF exhibits the (100) reflection at 2θ = 2.73°, which corresponds to the one-dimensional channel with a 32.4 Å diameter.[28] This peak is more pronounced in the two

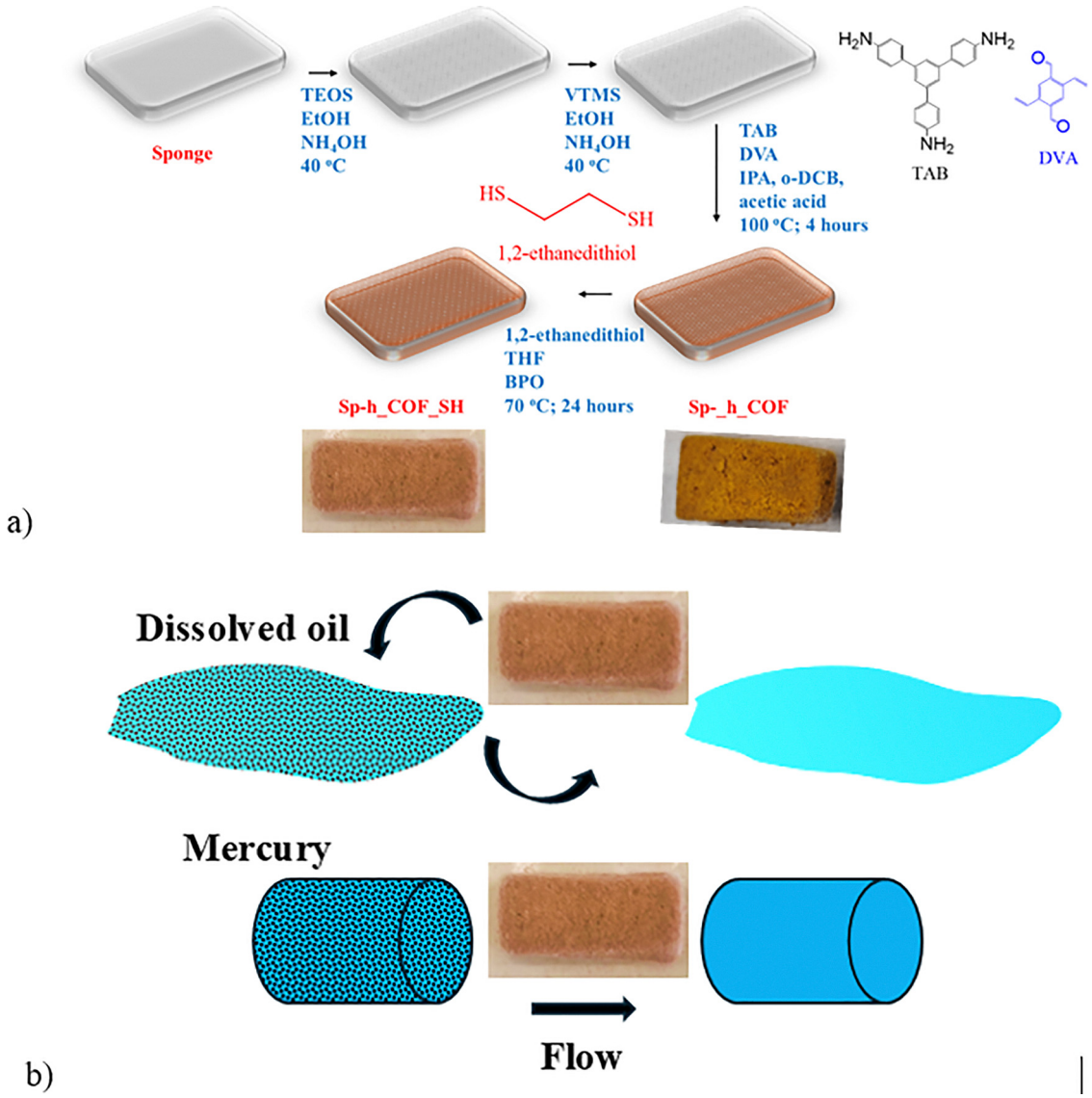

Fig. 1 (a) Schematic representation of the steps for the fabrication of the thiol (–SH) terminated sponges, alongside an image of the modified sponges and (b) the two main applications of sponges: dissolved oil removal under stirring and mercury absorption under continuous flow.

Table 1 A summary of sponge-based adsorbers for water-remediation technologies

Functional material	Application	Capacity	Ref.
Imine COF	Various oils	For silicone oil 150 g g^{-1}; for toluene 125 g g^{-1}	4
Organosilane	Various oils	70–120 g g^{-1}	7
MnO_2/wood	Heavy metals	—	11
Silicone sponge	Mercury	941.3 mg g^{-1}	13
Reduced graphite oxide	Copper	—	14
Triazine COFs	Copper	0.293 mg cm^{-2}	16
Magnetic NPs and vinyl-terminated silica	Crude oil and heavy metals	60–100 g g^{-1} for crude oil; 20.3–20.5 g g^{-1} for mercury and arsenic	22
Vinyl-terminated silica	Oil	60–100 g g^{-1}	24

control samples, especially in the Powder_ctrl, due to the hindering effect of the sponges in the formation of a highly ordered, crystalline, framework. In comparison, the Sp_h_COF_SH samples did not demonstrate any pronounced diffraction peaks at low angles, due to a symmetry collapse after the thiol functionalization. The 28.73° peak arises from the melamine sponge.[16]

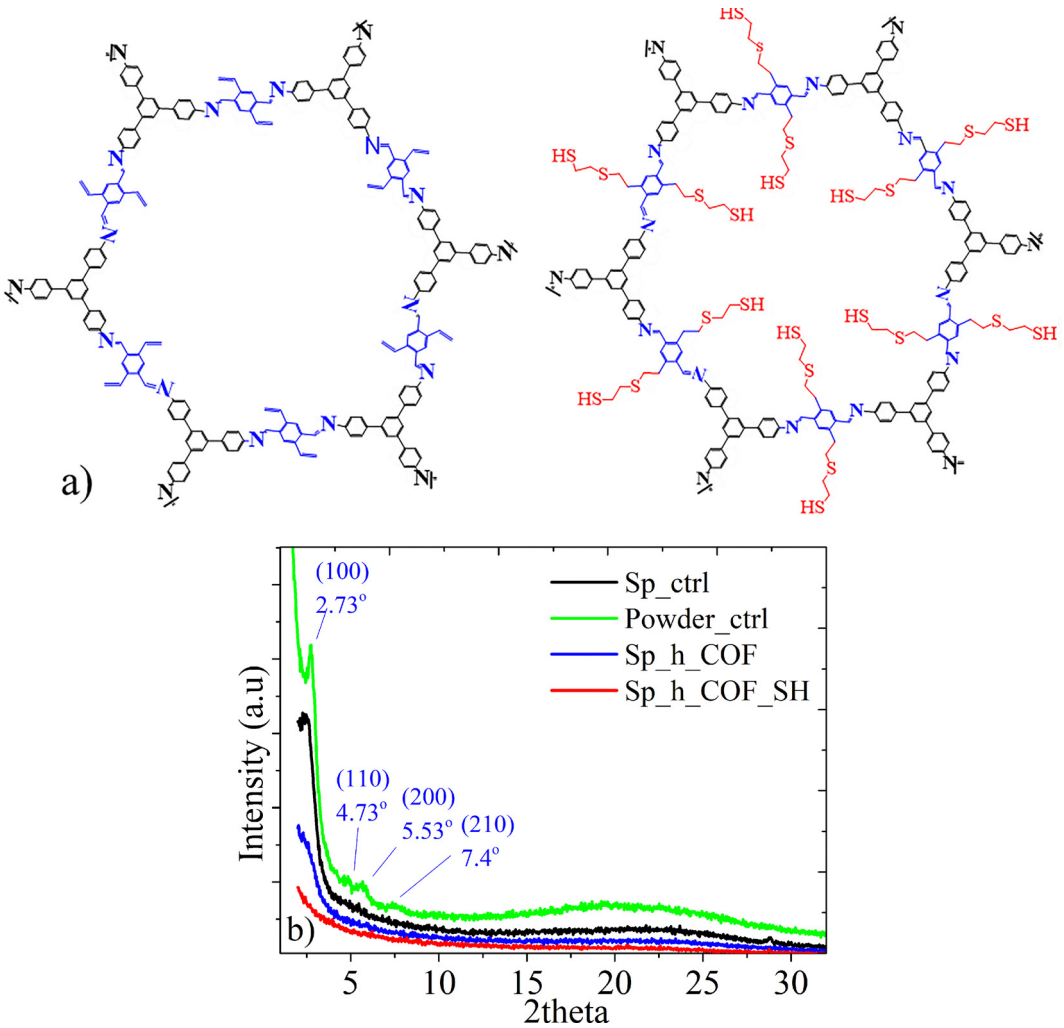

Fig. 2 (a) The chemical structure of the covalent organic framework with the pendant thiol groups and (b) the XRD patterns of Sp_h_COF, Sp_h_COF_SH and the control samples.

4.2. Evaluation of the stability of the modified sponges during the oil removal process

The sponge-based materials were initially evaluated as adsorbers for crude oil dissolved in deionized water. Representative images of the Sp_h_COF and Sp_h_COF_SH sponges added in the emulsions can be seen in Fig. 3. The dimensions of the two materials were 1.8 × 1.2 × 0.5 cm^3 and 1.4 × 1 × 0.5 cm^3, respectively. Before and after the oil removal, a detailed characterization of the materials was conducted to determine their stability and reusability, since both aspects are crucial for real-life applications. As a first step, the density of the materials was calculated. The results are gathered in Table 2, where an increase of the density of the sponges is observed, after the functionalization reactions. An apparent decrease of the density takes place after the first cycle of the dissolved oil sorption, because of the removal of the weakly bound organic moieties during the oil take-up and clean-up procedure with the organic solvents. More specifically, the pristine sponge is an ultra-light, porous material with a density of 8.5 mg cm^{-3}. After its decoration with hydrophobic silica groups and the covalent organic framework that largely filled the available pores of the melamine substrate, the density was massively increased at 51.5 mg cm^{-3}. Furthermore, the modification with 1,2-ethanedithiol led to an approximate twofold increase of the density, which was calculated at 114 mg cm^{-3}. After each oil adsorption and desorption cycle, even if the density decreased due to the removal of the weakly attached organic frameworks, it remained significantly higher than that of the pristine melamine sponge. The density of the COF-modified materials is also significantly higher compared to the density that we reported for hydrophobic sponges embedded with iron oxide nanoparticles in our previous work, which was at the level of 10.5–14.2 mg cm^{-3}.[22]

The morphology of the modified sponges was evaluated through SEM analysis. The SEM images of the hydrophobic sponge (Sp_h) are published in our previous work.[16] The SEM captures of the Sp_h_COF sample are presented in Fig. 4a at three different magnifications. The characteristic fibrillar network of the melamine sponge appears covered with the organic

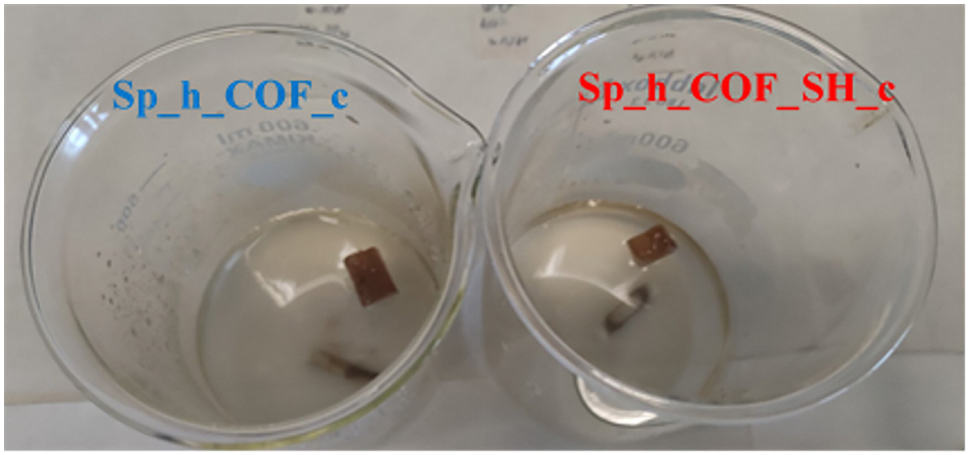

Fig. 3 Images of the sponges during the 1st oil adsorption cycle in a batch reactor under constant stirring with a magnet.

framework, while the dense network forms large agglomerates, intercalated between the fibers of the sponge. After three cycles of dissolved oil removal and clean-up procedure, it is qualitatively observed that a minor part of the weekly bound physisorbed COFs is removed (Fig. 4b), which is additionally supported quantitatively by the decline in density. A similar pattern is observed between the Sp_h_COF_SH and Sp_h_COF_SH_3c samples as well. After the functionalization with the 1,2-ethanedithiol, their morphology remained the same with the network lined up in large aggregates, intercalated between the channels of the melamine sponge (Fig. 4c). However, Sp_h_COF_SH_3c clearly demonstrates a reduced loading of the organic framework agglomerates (Fig. 4d). This indicates that after the oil adsorption and the subsequent purification process, the thiol-modified frameworks that were physiosorbed on the melamine are removed. These findings coincide well with the calculations performed for the reduced density values, outlined in Table 2.

EDS was employed to qualitatively and quantitatively identify the composition of the adsorbers. The focus is shed upon the thiol-terminated sponges before and after the oil adsorption process, since this is the system with the superior performance in the water remediation tests, as it will be discussed in the following sections of the present work. The representative EDS spectra can be seen in Fig. 5a, while the atomic and weight percentages derived from two different regions are shown in Fig. 5b and c and summarized in Table S1. The weight and atomic percentages of sulphur are reduced from 14.92 and 6.73% to 7.88 and 3.34%, indicating that a fraction of weakly physisorbed COFs is removed during the sorption cycles. However, it unambiguously proves that the thiol groups remain in a reasonably large percentage even after three oil removal cycles, which demonstrates the potential of the material in real-life applications.

Table 2 Density (in mg cm^{-3}) of the pristine sponge and the two COF-modified samples before and after the oil sorption and clean-up process

Density (mg cm^{-3})	Sponge	COF-functionalized sponge	COF–thiol functionalized sponge
Initial	8.5	51.5	114.0
After cycle no. 1	N/A	34.9	37.3
After cycle no. 3	N/A	24.8	23.4

To further evaluate the influence of the adsorption and desorption oil procedures upon the material, we examined the functionalized sponges through diffuse reflectance and UV-visible spectroscopy. Their respective diffuse reflectance spectra are demonstrated in Fig. S1 and by considering a direct band gap[29] for the covalent organic frameworks, the Tauc-plots are obtained and presented in Fig. 6, along with the derived energy band gaps. The Sp_h_COF exhibits a band gap of 2.38 eV, which remains practically the same after the 3rd cycle of adsorption, with Sp_h_COF_3c at 2.43 eV. An important enhancement of the gap from 2.38 eV of the Sp_h_COF to 2.46 eV with the successful thiol termination in Sp_h_COF_SH is demonstrated due to the presence of non-conjugated aliphatic chains of the thiol. Finally, only a minor increase in the band gap till 2.56 eV is observed for Sp_h_COF_SH_3c, most likely due to the presence of the non-conjugated oil contaminants. These values greatly match those reported in the literature for imine-linked COFs.[30] A similar increase of the band gap upon methylation of the side chains has been previously observed by Dautzenberg *et al.* for a series of COFs,[30] where their band gaps fluctuated in the range of 2.54–2.93 eV. These observations prove that the COF remains intact during the multi-cycle oil adsorption process.

The wetting behavior of the functionalized sponges was carefully evaluated through contact angle measurements. Representative images of the three samples with a water drop on their surface can be seen as an inset in Fig. 7, showing their intense orange-brown color and their texture. In Fig. 7, the contact angle images are presented for the Sp_COF and Sp_COF_SH samples before and after the first and third cycle of oil adsorption and desorption. The as-made Sp_h_COF and Sp_h_COF_SH samples demonstrate a strikingly different behavior, with the former having a hydrophobic character with a contact angle of 129°, while the latter has a hydrophilic

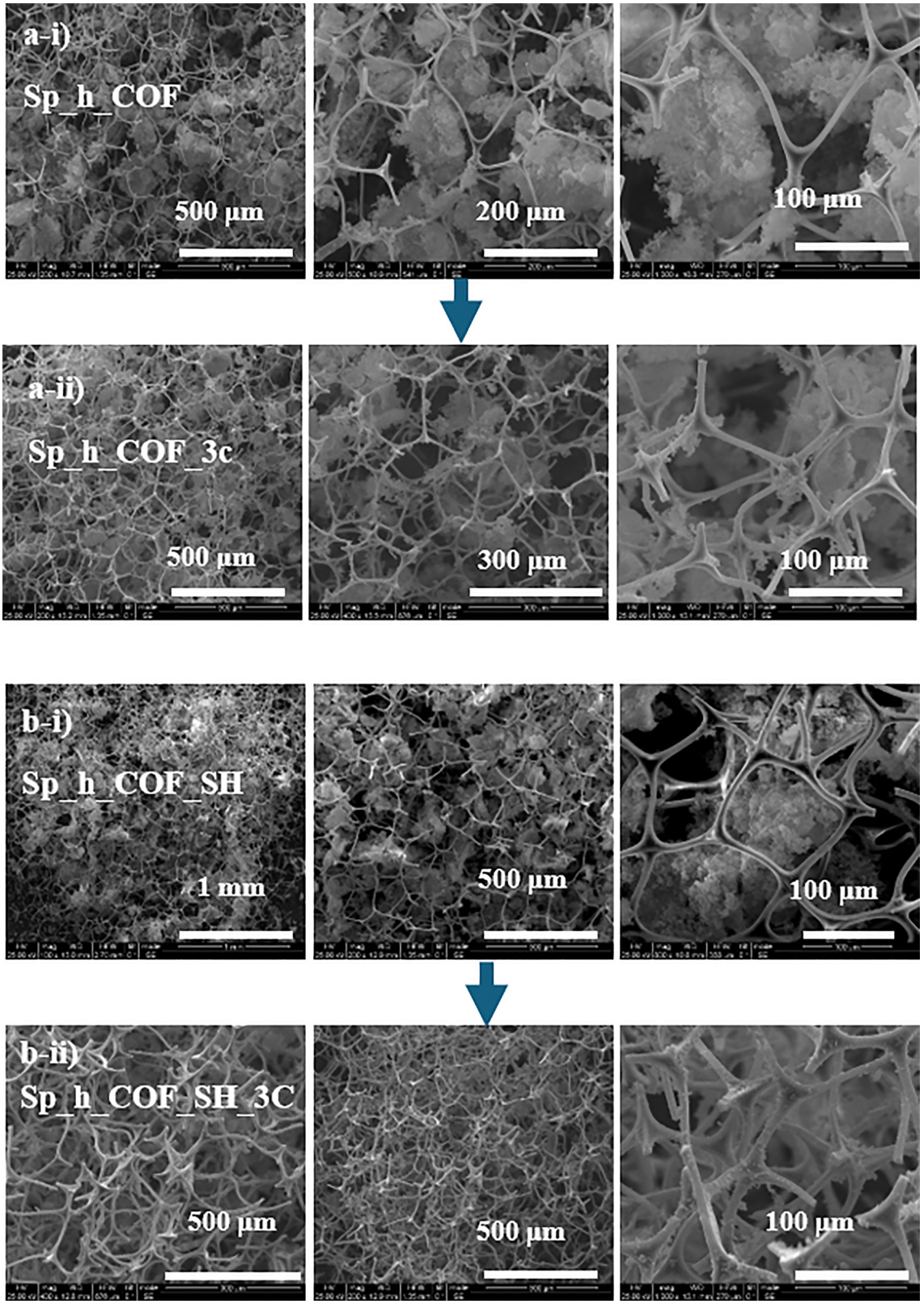

Fig. 4 SEM images of (a) Sp_h_COF (i) and Sp_h_COF_3c (ii); (b) Sp_h_COF_SH (i) and Sp_h_COF_SH_3c (ii).

behavior. However, a superhydrophilic response after a modification with an –SH bond has already been demonstrated in fabrics due to a combination of change of the roughness, van der Waals forces, and weak hydrogen bonding with water. Li *et al.* compared the wetting behavior of water droplets on a pristine fabric and a thiol–ene/silica hybrid-decorated fabric.[31]

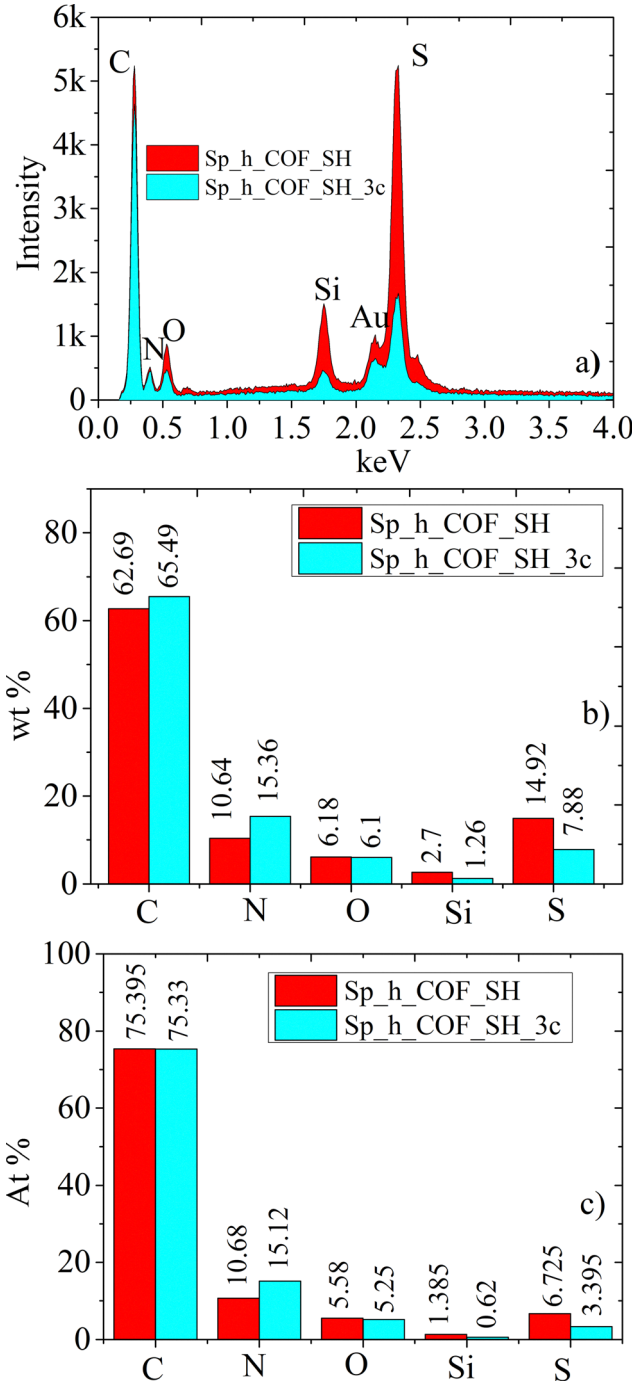

Fig. 5 (a) Representative EDS spectra of the thiol-modified sponges before (Sp_h_COF_SH) and after 3 cycles of oil removal (Sp_h_COF_SH_3c) and their wt% (b); at% (c). The data in (b) and (c) are the average of two different regions.

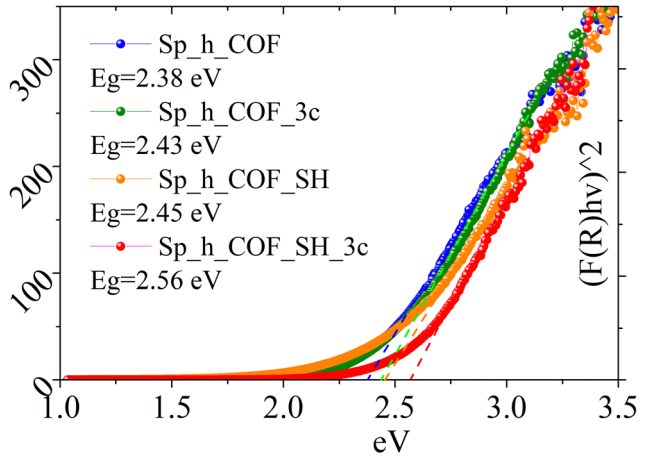

Fig. 6 Tauc-plots derived from the diffuse reflectance spectra of Fig. S1 for the following samples: Sp_h_COF; Sp_h_COF_3c; Sp_h_COF_SH_3c. The band gaps are indicated in the plot.

The water droplets on the pristine fabric had a WCA of 86.4°, while on the thiol–ene/silica hybrid fabric, water permeated and spread out completely, notably, within 0.36 s. Similarly, in ref. 27 a drastic decline of hydrophobicity was observed, due to changes in the micro- and nano-roughness of their system. It is known that sulfur has a hydrophobic character, while –SH is more hydrophilic and polar due to its capacity to form H-bonds with water. Depending on the environment, redox conditions can convert the wetting behavior of –S-containing groups.[32] Thus, an amphiphilic character, dependent on the surrounding environment and protonation/deprotonation processes (from thiol to thiolate) may be activated. Following the oil adsorption and desorption cycles in this study, the sponges demonstrate hydrophobic behavior, with a contact angle reaching the value of 140.45° for the Sp_h_COF_SH_3c sample and 131.60° for Sp_h_COF_3c (Fig. 7c). In that case, the abundant hydrophobic characteristics of the interior layer in synergy with strongly adsorbed aliphatic or aromatic molecules from the crude oil led to the water-repelling characteristics, observed in the water drop experiments.[33] To further evaluate the hydrophobic/hydrophilic properties of the materials, a control experiment was conducted, where the COF powders were removed from the sponges with and without thiol groups, and were dispersed in water. The striking difference between a profound hydrophobic behavior in the powder without the thiol and a stable suspension in the powder with the thiol groups can be seen in Fig. S2.

Vibrational spectroscopy was applied to identify the structure of organic precursor molecules and polymers. The FTIR spectra of the synthesized Sp_h_COF and Sp_h_COF_SH samples before and after oil removal experiments are presented in Fig. S3 to demonstrate the successful synthesis and the chemical stability of the covalent organic frameworks on the hydrophobic sponges, and the spectra of the Tab and Dva precursors are presented in Fig. S3c. In Fig. 8, the spectra of the COF-functionalized sponges, Sp_h_COF, Sp_h_COF_SH, and Sp_h_COF_SH_3c are presented alongside the spectrum of the pristine sponge. The COF-functionalized sample demonstrates new peaks assigned to the –C=N– and –C=C– double bonds at 1591 and 1517 cm^{-1} (ref. 34) and the disappearance of the N–H (peaks at 3432 and 3352 cm^{-1}) related to the Tab as well as the modes at 2700–2780 cm^{-1} characteristic of the aldehyde hydrogen of Dva.[4] The peak at 1683 cm^{-1}, which is characteristic of the aldehyde carbon–oxygen double bond, is also present in the pristine sponge. In Fig. S3c, we compare the

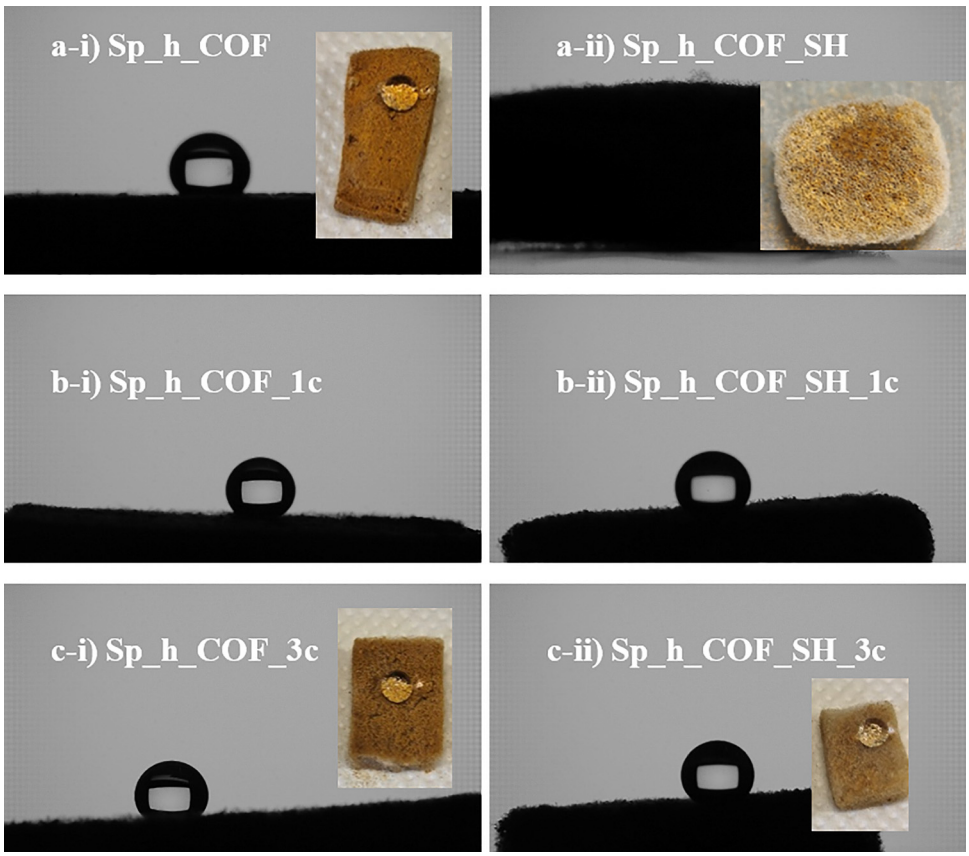

Fig. 7 Contact angle measurements for the Sp_h_COF (left-i) and the Sp_h_COF_SH (right-ii) sponges. (a) As-made samples (b) after one cycle of oil adsorption–desorption. (c) After three cycles. The images of the sponges with a water drop on their surface appear as insets.

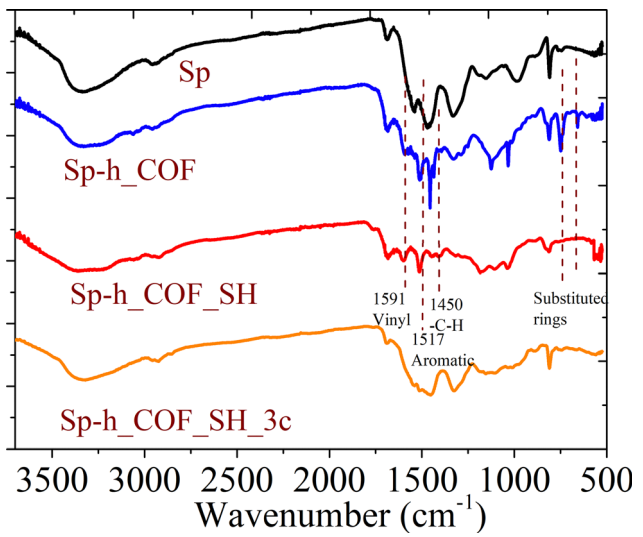

Fig. 8 FTIR spectra of Sp, Sp_h_COF, Sp_h_COF_SH and Sp_h_COF_SH_3c.

FTIR spectra of the pristine Tab and Dva precursors with that of the Sp_h_COF sample. While the peak intensity increases in the Sp_h_COF material, which signals some unreacted aldehyde, the rest of the spectrum is markedly different with the precursor molecules. After their functionalization with dithiol, the vibration peak of the –S–H bond rose in the 2500–2600 cm^{-1} region (Fig. S4) with a weak intensity. It is important to note that the characteristic peak of the S–H group is notoriously elusive[35] and, in general, exhibits a very low intensity due to the low polarity of the thiol group. In the case of the thiol-functionalized sample, after the third oil removal cycle, a significant intensity loss of the characteristic peaks assigned to the COF molecules is observed in the FTIR spectrum, which is in accordance with the fewer population of the agglomerates observed in SEM. The Raman spectra at green light excitation showed a fluorescence from all samples.

4.3. The adsorption mechanism for dissolved oil removal

In this subchapter, a comprehensive study on the kinetic model of adsorption regarding the dissolved oil and active sites of the thiol-terminated COF hydrophobic sponges is presented. Our experiment was performed utilizing a stock solution of a 100 ppm oil-in-water emulsion, as described in Section 2.5. The pH of the emulsion was 6.05. A representative video and image of the preparation of the emulsion can be seen in Fig. S5. Initially, the absorbance of emulsions ranging from 25 to 2000 ppm of oil was examined to identify the linear region of the absorbance

in our spectrometer. The representative graph alongside the image of the dispersions is presented in Fig. S6. The 100 ppm oil emulsion was kept under vigorous stirring in the presence of the sponge throughout the adsorption experiment. The functionalized sponges were added on the surface of the emulsion and aliquots of 2 mL volume were taken in specific time intervals. The aliquots were returned to the emulsion immediately after recording their UV-visible spectra.[36] The procedure can be seen in the video of Fig. S7, where the Sp_h_COF_SH sample is depicted. Finally, the efficiency in oil removal was quantitatively studied using straightforward optical absorption techniques. The adsorption capacity of the sponges was evaluated using the eqn (1).

$$q_e = \frac{\left(10 - 10 \cdot \frac{A}{A_0}\right)}{V} \quad (1)$$

where q_e is the fraction of adsorbed oil from the sponges (mg of oil per cm^3 of sponge; mg cm^{-3}), A is the absorbance measured in different time intervals, A_0 is the absorbance for t = 0 min corresponding to 10 mg of oil in the 100 mL of emulsion and V is the volume of the measured sponge.

In Fig. 9a, the decrease of the A/A_0 with time is presented for the Sp_h_COF and Sp_h_COF_SH samples, while the data regarding the pristine sponge are presented in Fig. S8. The visible light absorbance was recorded at selected time intervals for a period of 350 minutes, and the final measurement took place after 1440 minutes (24 hours). The Sp_h_COF_SH sample completely removed all the dissolved oil, in contrast to the Sp_h_COF sponge. The quantitative analysis clearly demonstrates the crucial role of the thiol functional group for effective oil adsorption. The pristine sponge absorbs mainly water and minor fractions of oil, while the COF-functionalized, hydrophobic sponge, removes oil following a linear decrease of the absorbance value. In contrast, the thiol-modified sponge demonstrates a rapid, exponential decrease of visible light absorbance, related to the oil removal. The Sp_h_COF_SH adsorption curve shown in Fig. 9b follows a first-order kinetic model and the fitting model using eqn (2).

$$\ln C_t = -k \cdot t + \ln C_0 \quad (2)$$

The linear fit, with an excellent adj-R-square = 1, results in a rate constant k = 0.01037 min^{-1} and an initial concentration C_0 = 92.5 ppm. The first-order kinetic model of the process indicates that all adsorption sites have equal energy and chemical properties.

In Fig. 9c, the adsorption capacity, q_m in mg cm^{-3}, of the Sp_h_COF and Sp_h_COF_SH samples for three subsequent oil adsorption and desorption cycles is demonstrated. Clearly, the exponential increase of q_m for the thiol-terminated COF is gradually reduced to a linear response after subsequent cycles. At the third cycle, both the pristine and the thiol-terminated samples present an identical behavior, which coincides well with the lower percentage of sulfur as demonstrated by the EDS analysis. In order to explain these results, we examine the

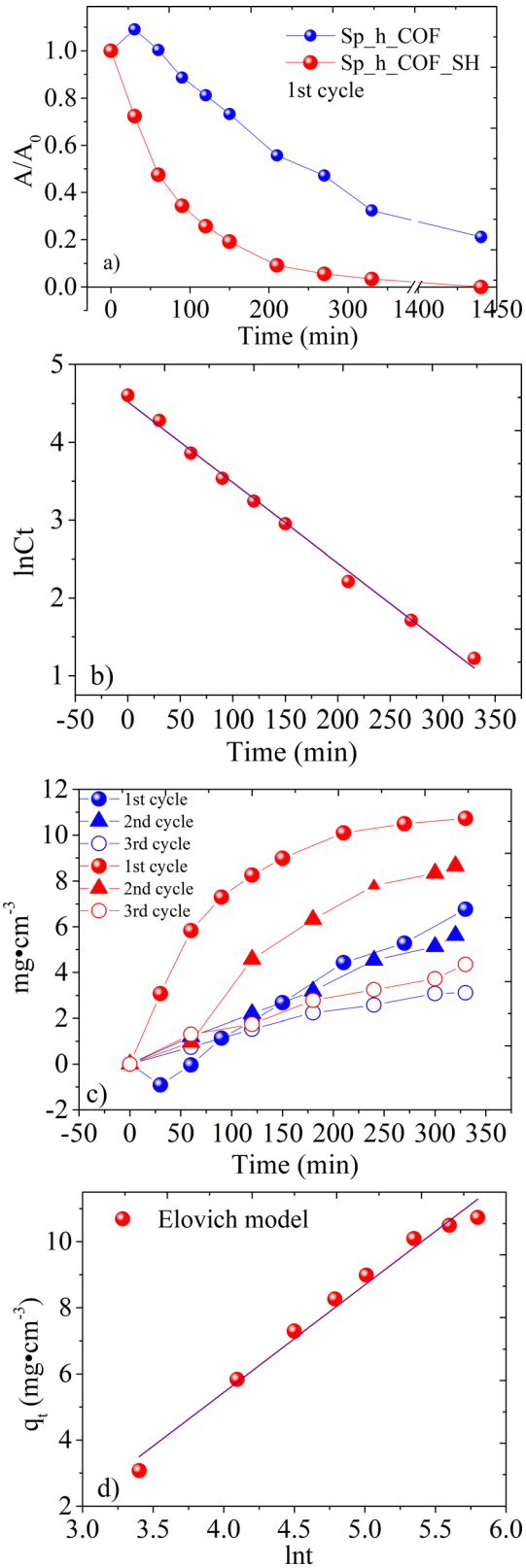

Fig. 9 (a) The decrease of the oil absorbance at 700 nm (A) with respect to the initial value (A_0) for the two composite sponges, (b) first-order kinetic fitting for the Sp_h_COF_SH sample, (c) kinetic adsorption graphs for the Sp_h_COF (blue curves) and Sp_h_COF_SH (red curves) for the 1st, 2nd and 3rd runs of oil adsorption and desorption and (d) the Elovich fitting model for Sp_h_COF_SH representing the first oil removal cycle.

composition of the crude oil. Crude oil itself contains sulfur, thiols, as well as metals that have a high affinity with the –S–H group.[37,38] Furthermore, the functionalization with 1,2-ethanedithiol inherited the sponges with two additional hydrocarbon groups. Hence, we assign the high efficiency of the Sp_h_COF_SH sample to the combination of the above-mentioned factors.

Additionally, the kinetics of the adsorption were described through a widely used equation, which represents the Elovich model. The equation of the Elovich kinetic model is described using the following equation:

$$q_t = \frac{1}{a}\ln(\alpha \cdot \beta) + \frac{1}{a} \cdot \ln(t) \quad (3)$$

where q_t (mg cm^{-3}) is the adsorption capacity in each time interval, t is the time (min), α is the initial adsorption rate, and β is the desorption constant. The Elovich model describes the adsorption kinetics considering the chemisorption mechanism, where the adsorption rate decreases exponentially as the adsorbed amount increases. It describes activated adsorption, where the reaction occurs at localized sites and leads to a decrease in rate as the active sites become occupied.[39] This is assigned to the heterogeneous nature of solid surfaces and the increase in occupied active sites. The obtained parameters of the initial rate α and desorption constant β indicate strong attachment and surface irregularities, respectively. The excellent fitting with adj-R square = 0.983 indicates a surface with varied active binding sites, where the most efficient sites are filled first, rapidly, slowing and hindering the overall rate (Fig. 9d). A second-order kinetic fitting was also applied and presented a non-linear growth rate (Fig. S9).[40]

In general, crude oil sorption is a complex process involving physisorption through weak van der Waals forces, strong chemical interactions (*i.e.* chemisorption) through the functional groups of the organic molecules and sulfur and metal components and pore diffusion, with the latter being in general the rate-determining step.[41,42]

The linear fitting using the Elovich model provides the following values: α = 0.307 mg cm^{-3} min^{-1} and β = 0.323 g cm^{-3}. The α parameter represents the initial adsorption rate and indicates how quickly the adsorption process begins, while the β constant is related to the extent of surface coverage and the activation energy for the sorption.[43] Additionally, the data were fitted using the Bangham model, a diffusion kinetic model of substances within the pores of the adsorbent while a reaction happens at the liquid/solid interface. The Bangham model with an adj-R square = 0.9, in Fig. S10, indicates that the mass transfer is limited and diffusion is not the rate-determining step.

4.4. Mercury removal from the aqueous solution

The design and synthesis of functional materials with high selectivity and sensitive detection are crucial for contemporary environmental science and its applications. Terminal groups are introduced in porous materials to render them suitable for the chemisorption of metallic cations. Typical characteristic groups that decorate both metal organic and covalent organic frameworks and other porous media include thiol, oxime, and thiourea functional groups, containing S, N, or both N and S elements. These groups enable the ultra-efficient complexation of cations such as Pb^{2+} and Hg^{2+}. For Hg^{2+}, a record-breaking adsorption capacity (957.94 mg g^{-1}, 1.99 times that of unmodified materials) and distribution coefficient (743 333 mL g^{-1}) have been observed for functionalized metal–organic frameworks such as the well-known MOF 808.[44]

The metal removal capacity of the composite sponges was evaluated under dynamic adsorption experiments, which are considered closer to real-life applications compared to static experiments. As a control experiment, the functionalized sponge with the imine COF was studied initially prior to the thiol modification. These nitrogen-rich COFs have been previously demonstrated to be efficient absorbers for mercury cations.[45] For the experiments of this study, an aqueous solution of mercury nitrate and a multielement standard solution that contains 27 different elements were utilized. The pH of mercury nitrate and of the multielement solution was 3.5 and 1, respectively. It is considered that the pH greatly influences mercury behavior and its solubility in water. At very low, acidic pH levels, mercury is predominantly in the form of "free" divalent cations, *i.e.* Hg^{2+}. As the pH levels increase, the hydroxide $HgOH^-$ form dominates. Thus, the dominant mercury species in the solution are Hg^{2+} at pH < 3.0, and $Hg(OH)_2$ at pH > 5 and both species alongside $HgOH^+$ co-exist between pH 3 and pH 5.[46,47] This is outlined in the chemical equations that can be seen below.

$$Hg^{2+} + OH^- \leftrightarrow HgOH^+ \quad K_3 = 10^{10.6} \quad (4)$$

$$HgOH^+ + OH^- \leftrightarrow Hg(OH)_2 \quad K_4 = 10^{11.2} \quad (5)$$

$$Hg(OH)_2 + OH^- \leftrightarrow Hg(OH)_3{}^- \quad K_5 = 10^{-0.9} \quad (6)$$

In dilute solutions, the mercury species at different pH values are calculated according to the above equilibrium constants, and are denoted as α'_0, α'_1, α'_2 and α'_3. They represent the percentages of $Hg_2{}^+$, $HgOH^+$, $Hg(OH)_2$ and $Hg(OH)_3{}^-$, respectively, following the trend seen in Fig. 10a.

$$\alpha'_0 = 1/\left[K_3 \cdot [OH^-] + K_3 \cdot K_4 \cdot [OH^-]^2 + K_3 \cdot K_4 \cdot K_5 \cdot [OH^-]^3\right] \quad (7)$$

$$\alpha'_1 = \alpha'_0 \cdot K_3 \cdot [OH^-] \quad (8)$$

$$\alpha'_2 = \alpha'_0 \cdot K_3 \cdot K_4 \cdot [OH^-]^2 \quad (9)$$

$$\alpha'_3 = \alpha'_0 \cdot K_3 \cdot K_4 \cdot K_5 \cdot [OH^-]^3 \quad (10)$$

In the experiments, we observed a drastically different behavior of the Sp_h_COF sample, where almost no mercury uptake was observed in the mercury nitrate solution, while a rapid and more efficient removal was achieved at the multielement solution (Fig. 10b). As the pH of the mercury nitrate solution is 3.5 and of the multielement solution is highly acidic

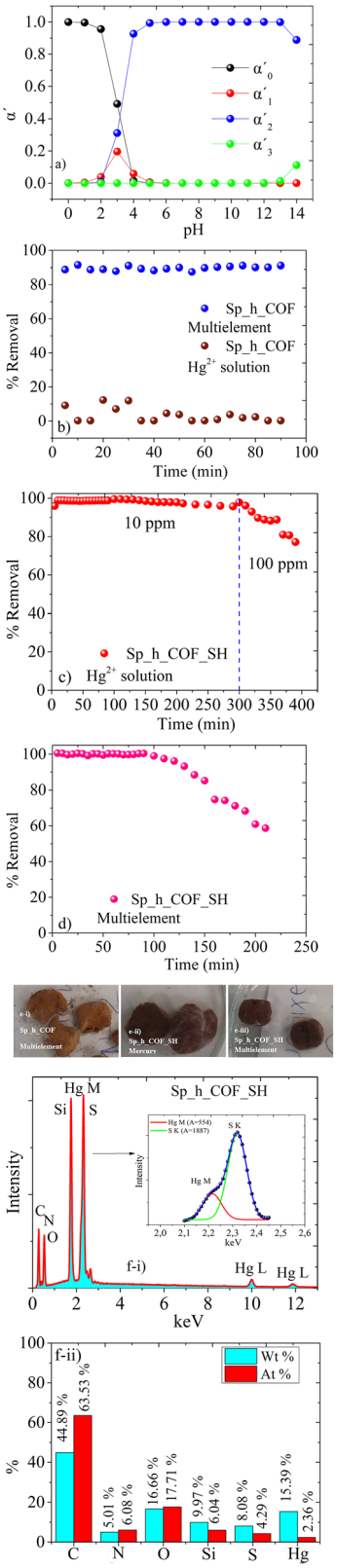

Fig. 10 (a) The fractions of Hg^{2+}, $HgOH^{+}$, $Hg(OH)_2$ and $Hg(OH)_3^{-}$ for pH levels from 0 to 14. Dynamic adsorption experiments for Sp_h_COF (b; blue: multivalent solution; cyan: divalent mercury solution), Sp_h_COF_SH (c; divalent mercury) and Sp_h_COF_SH (d; multivalent solution). (e) Images of the three samples after the experiment. (f) EDS spectrum (i) and the quantitative analysis graph (ii) for the Sp_h_COF_SH sample after the dynamic adsorption of mercury.

with a pH = 1, and we assign this discrepancy to the inactivity of the nitrogen moieties to the successfull coordination with $HgOH^{+}$ in contrast with the divalent cation. The efficiency of the system in sequestering mercury is determined by the delicate balance between metal speciation and the protonation state of the imine linkages. At pH 1, mercury exists primarily as the free mercuric ion Hg^{2+}, which acts as a potent and "soft" Lewis acid. Due to its high polarizability, Hg^{2+} tends to withdraw electron density from the imine N═C bond, even when the nitrogen is already protonated RN═CR–H^{+}. At pH 1, complete protonation of the imines strongly polarizes the N═C bond, creating an electronic environment conducive to Hg^{2+} entry. Mercury coordinates with nitrogen, while the framework architecture keeps the carbon protected from water-induced hydrolysis. The free, "softer" Hg^{2+} form allows interaction with the double bonds of the COF. These interactions stabilize the metal within the lattice. Conversely, at pH 3.5, the emergence of $[Hg(OH)]^{+}$, a "harder" Lewis acid, and the lack of full imine protonation limit the binding affinity.[48]

Following the soft and hard acid–base theory, sulfur-containing groups are excellent candidates for the removal of mercury from aqueous solutions. Mercury, particularly in forms like Hg^{2+} and methylmercury, is classified as a soft Lewis acid. This large cation with a low charge density is highly polarizable. Sulfur-containing compounds, such as sulfides (S^{2-}) and thiolates (SH^{-}), are highly polarizable with a low electronegativity, and thus are classified as soft Lewis bases. With respect to the above, mercury has a high affinity for sulfur, leading to the formation of very stable, insoluble complexes. The reaction thermodynamics prove the high affinity of mercury to sulfur (*i.e.*, $\log K \approx 52.7$–53.3) compared to that for Hg to organic matter (*i.e.*, $\log K = 22$–28).[49] Under the dynamic, continuous flow conditions the Sp_h_COF_SH samples presented a complete removal of mercury for 300 minutes when the solution had a concentration of 10 ppm (Fig. 10c). We then switched to a 100 ppm solution where a partial saturation of the capacity was observed. The material reached saturation much earlier when a multielement solution was applied (Fig. 10d) due to competition from other metal cations. Specifically, we identified the removal of lead during the experiments with the multi-element solution. A detailed study focusing on the competition between the different heavy metals, specifically on the Pb^{2+}, would be a subject of a separate work.

In Fig. 10e, we present the images of the sponges after the dynamic experiments, where it is worth noting that the Sp_h_COF_SH sample retained its hydrophilicity with the water droplet readily spreading on its surface. The thiol-terminated sponges obtained a darker color after mercury adsorption in both single element and multi-element systems. Additionally, EDS analysis proved the presence of both sulfur and mercury, with the characteristic Hg L peaks appearing at high energies, while the Hg M and the S K peaks overlap, as expected (Fig. 10f). In the inset graph added in Fig. 10f-i, the deconvolution reveals the two distinctive peaks at 2.2 keV for the Hg and 2.3 keV for the S element. Fig. 10f-ii demonstrates the respective quantitative analysis and reveals an atomic percent of 4.29% for the

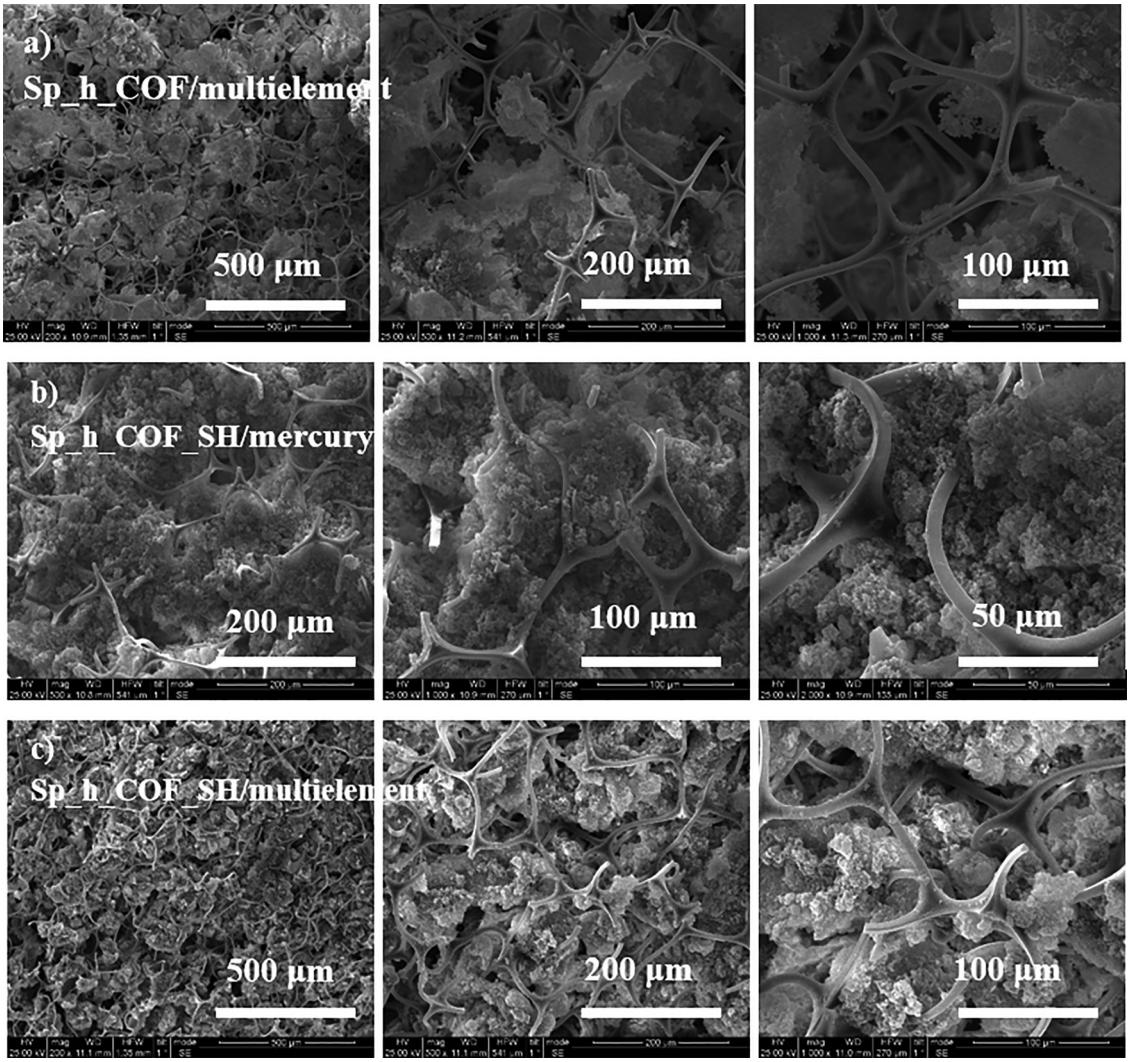

Fig. 11 SEM images of the sponges after the heavy metal dynamic adsorption (a) Sp_h_COF/multielement solution (b) Sp_h_COF_SH/mercury solution (c) Sp_h_COF_SH/multielement solution.

sulfur element and 2.36% for mercury (see also Table S2). Before Hg(II) adsorption, the system contains higher percentages of C, N, and S elements than after the adsorption experiments, which is consistent with the physisorbed quantities drifted by the flow of the solution. Although Sp_h_COF_SH contains lower amounts of O and Si in comparison to the aftermath values of the dynamic adsorption experiment, Si values may be increased due to the exposure of the hydrophobic layer following the removal of the physisorbed molecules by solution flow, while O has its source from the $Hg(NO_3)_2$ aqueous solution. The SEM images of the three systems after the heavy metal removal application are presented in Fig. 11. It appears that the materials remained practically the same, which further strengthens their positive aspects for everyday and industrial applications. The Sp_h_COF_SH after mercury adsorption (Fig. 11b) presents a more continuous bonded network in comparison to the initial agglomerates.

5. Conclusions

In conclusion, we present the synthesis, characterization, stability evaluation, and application of thiol-functionalized imine COFs on commercial melamine sponges as adsorbers for the removal of dissolved oil and mercury. The *in situ* Schiff-base condensation of the precursors took place upon the hydrophobic sponges and the crucial thiol–ene coupling reaction of the COF were demonstrated through EDS and FTIR spectroscopy; their structure and morphology were characterized by XRD and SEM during all the synthesis steps. The critical role of the thiol group in determining the efficiency of the material in water remediation was demonstrated through dynamic adsorption experiments, and a quantitative analysis was performed using UV-visible and ICP–OES techniques. The oil adsorption follows a first-order kinetic mechanism with different active sites, with a rapid exponential decay of capacity. The sponges present excellent removal efficiency of highly toxic metals such as

mercury in dynamic adsorption experiments. The thiol-terminated COF exhibited an excellent removal efficiency of 77–99% in 5-minute interval measurements of dynamic flow of 10 and 100 ppm solutions. The selective adsorption of mercury is highlighted throughout multiple cycles in the presence of 27 competitive elements. By tailoring the coverage of the sponge with the COF, a material with a high cost of preparation, the system will find its way in real-life applications with respect to its efficiency and stability in consecutive experiments under dynamic conditions.

Author contributions

P. B.: conceptualization, methodology, formal analysis, investigation, data curation, and writing – original draft and review and editing. N. T.: conceptualization, methodology, formal analysis, investigation, data curation, and writing – original draft. M.-A. G.: methodology, investigation, and data curation. T. L.: methodology, investigation, writing original draft, and data curation. L.-A. T.: methodology, investigation, writing original draft, and data curation. D. T.: visualization, project administration. A. K.: methodology and investigation. N. Z.: methodology and investigation. E. S.: methodology and investigation. T. S.: supervision and project administration. E. A. P.: methodology, investigation, and supervision. P. D.: conceptualization, methodology, formal analysis, investigation, writing – original draft, supervision, visualization, and project administration.

Conflicts of interest

The authors declare that there is no conflict of interest.

Data availability

Data for this article are either included in the manuscript or are available from the corresponding authors upon request.

Supplementary information (SI): Fig. S1: diffuse reflectance spectra. Fig. S2: COF powders with and without thiol were removed mechanically from the sponges and dispersed in water. Fig. S3: video and photo of the preparation of the oil/water emulsion using a high-share emulsifier. Fig. S4: FTIR spectra. Fig. S5: image and video of the preparation of the emulsion. Fig. S6: The reference emulsions and the corresponding calibration curve. Fig. S7: video of the first oil removal cycle using the thiol-functionalized sponge. Fig. S8: Oil adsorption curve of the pristine sponge. Fig. S9: Second order kinetic model. Fig. S10: Bangham model graph. Tables S1 and S2: Quantitative EDS analysis data. See DOI: https://doi.org/10.1039/d6ma00413j.

Acknowledgements

We acknowledge the support from the project ''ATTP4 0359579'' COF4SEA'' (MIS 5217185), co-financed by the European Union and Greek National Funds through the Operational Program ATTIKA 2014–2020, under the call ''Research and Innovation Cooperations in the Region of Attica''.

References

1 United States Environmental Protection Agency, Understanding Oil Spills And Oil Spill Response, 540-K-99-007 OSWER 9200.5-104A PB2000-963401, December 1999.
2 K. Sharma, G. Shah, K. Singhal and V. Soni, Comprehensive insights into the impact of oil pollution on the environment, *Reg. Stud. Mar. Sci.*, 2024, **74**, 103516.
3 Y. Feng and J. Yao, Design of Melamine Sponge-Based Three-Dimensional Porous Materials toward Applications, *Ind. Eng. Chem. Res.*, 2018, **57**(22), 7322–7330.
4 J. Li, Y. Yang, W. Ma, G. Li, Q. Lu and Z. Lin, One-pot room-temperature synthesis of covalent organic framework-coated superhydrophobic sponges for highly efficient oil-water separation, *J. Hazard. Mater.*, 2021, **411**, 125190.
5 B. Dai, Y. Ding, C. Chen, L. Shen, D. L. Zhao, Y. Jiao, H. Lin and Y. Xu, Super-hydrophilic membranes fabricated by synergistic integration of covalent organic framework nanoflowers and hydrophilic layers for efficient oil-water separation, *Desalination*, 2024, **592**, 118095.
6 D. Cong, Q. Li, B. Zhao, L. Wang, W. Kan, B. Liu, F. Bu and Y. He, Fluorine-free self-hydrophobic covalent organic framework for unidirectional oil-water and emulsion separation, *Colloids Surf., A*, 2025, **725**, 137711.
7 W. Zhang, X. Zhai, T. Xiang, M. Zhou, D. Zang, Z. Gao and C. Wang, Superhydrophobic melamine sponge with excellent surface selectivity and fire retardancy for oil absorption, *J. Mater. Sci.*, 2017, **52**(73), 85.
8 Q. Sun, B. Aguila, J. A. Perman, T. Butts, F.-S. Xiao and S. Ma, Integrating Superwettability within Covalent Organic Frameworks for Functional Coating, *Cell*, 2018, **4**(7), 1726.
9 B. Fei-Baffoe, E. Badu, K. Miezah, L. N. A. Sackey, A. Sulemana, E. Ebo and Y. Amuah, Contamination of groundwater by petroleum hydrocarbons, *Heliyon*, 2024, **10**, e25924.
10 C. Morosini, E. Terzaghi, G. Raspa, E. Zanardini, S. Anelli, S. Armiraglio, E. Petranich, S. Covelli and A. Di Guardo, Mercury vertical and horizontal concentrations in agricultural soils of a historically contaminated site: Role of soil properties, chemical loading, and cultivated plant species in driving its mobility, *Environ. Pollut.*, 2021, **285**, 117467.
11 S. V. Saghir and E. K. Goharshadi, Multifunctional MnO2 nanorods-modified wood sponge for water remediation: applications for heavy metal sorption and oil/water separation, *Wood Sci. Technol.*, 2024, **58**, 2097–2113.
12 S. A. Ali and M. A. J. Mazumber, A new resin embedded with chelating motifs of biogenic methionine for the removal of Hg(II) at ppb levels, *J. Hazard. Mater.*, 2018, **350**, 169–179.
13 J. Cao, Y. Wang, D. Wang, R. Sun, M. Guo, S. Feng and A. Super-Amphiphilic, 3D Silicone Sponge with High Porosity for the Efficient Adsorption of Various Pollutants, *Macromol. Rapid Commun.*, 2021, **42**, 2000603.

14 H. Zhu, D. Chen, S. Yang, N. Li, Q. Xu, H. Li, L. Wang, J. He, J. Jiang and J. Lu, A versatile and cost-effective reduced graphene oxide-crosslinked polyurethane sponge for highly effective wastewater treatment, *RSC Adv.*, 2016, **6**, 38350.

15 L. Wang, J. Li, Q. Jiang and L. Zhao, Water-soluble Fe_3O_4 nanoparticles with high solubility for removal of heavy-metal ions from wastewater, *Dalton Trans.*, 2012, **41**, 4544–4551.

16 P. Bika, N. Ioannidis, P. Tsipas, S. Papagiannis, M.-A. Gatou, E. A. Pavlatou, A. G. Karydas, T. Stergiopoulos and P. Dallas, Detection and Selective Sorption of Copper Ions by a COF-Modified Melamine Sponge, *ACS Omega*, 2025, **10**, 21755–21766.

17 P. Bika, N. Ioannidis, M.-A. Gatou, Y. Sanakis and P. Dallas, Copper Coordination and the Induced Morphological Changes in Covalent Organic Frameworks, *Langmuir*, 2022, **38**, 3082–3089.

18 P. Das and S. K. Mandal, In-depth experimental and computational investigations for remarkable gas/vapor sorption, selectivity, and affinity by a porous nitrogen-rich covalent organic framework, *Chem. Mater.*, 2019, **31**, 1584–1596.

19 C. Arqueros, L. Welte, C. Montoro and F. Zamora, Imine-based covalent organic framework gels for efficient removal of Fe^{2+} from contaminated water, *J. Mater. Chem. A*, 2024, **12**, 20121–20128.

20 T. Chen, W.-N. Jiao, W.-D. Zhu, H. Wang, S. Huang, X.-C. Lin, J. Liu, H.-S. Xu and C.-Y. Su, Designed Synthesis of Imine-Linked 2D Covalent Organic Frameworks with Enhanced Stability and Functionality, *Chem. Mater.*, 2024, **36**(15), 7362–7369.

21 Q. Sun, B. Aguila, J. Perman, L. D. Earl, C. W. Abney, Y. Cheng, H. Wei, N. Nguyen, L. Wojtas and S. Ma, Post-synthetically Modified Covalent Organic Frameworks for Efficient and Effective Mercury Removal, *J. Am. Chem. Soc.*, 2017, **139**, 2786–2793.

22 P. Bika, N. Todorova, M.-A. Gatou, M. Pissas, E. Devlin, E. Sakellis, N. Boukos, N. Lagopati, T. Lymperopoulou, L.-A. Tsakanika, E. A. Pavlatou, V. K. Tzitzios and P. Dallas, Magnetically controllable sponges for crude oil, mercury, and arsenic removal, *Environ. Sci.: Nano*, 2026, **13**, 280–295.

23 M. H. Tai, J. Juay, D. D. Sun and J. O. Leckie, Carbon–silica composite nanofiber membrane for high flux separation of water-in-oil emulsion – Performance study and fouling mechanism, *Sep. Purif. Technol.*, 2015, **156**, 952.

24 H. Gao, P. Sun, Y. Zhang, X. Zeng, D. Wang, Y. Zhang, W. Wang and J. Wu, Two-step hydrophobic fabrication of melamine sponge for oil absorption and oil/water separation, *Surf. Coat. Technol.*, 2018, **339**, 147–154.

25 X. Jiang, X. Tang, L. Tang, B. Zhang and H. Mao, Synthesis and formation mechanism of amorphous silica particles via sol–gel process with tetraethylorthosilicate, *Ceram. Int.*, 2019, **45**, 7673–7680.

26 G. O. Kayan and I. Akin, Ti_3SiC_2 MAX phase: Sol–gel processing, characterization, and sinterability, *J. Am. Ceram. Soc.*, 2026, **109**(1), e70341.

27 X. Li, C. Zhang, S. Cai, X. Lei, V. Altoe, F. Hong, J. J. Urban, J. Ciston, E. M. Chan and Y. Liu, Facile transformation of imine covalent organic frameworks into ultrastable crystalline porous aromatic frameworks, *Nat. Commun.*, 2018, **9**, 2998.

28 C. Miao, X. Xun, L. J. Dodd, S. Niu, H. Wang, P. Yan, X.-C. Wang, J. Li, X. Wu, T. Hassell and Z.-J. Quan, Inverse Vulcanization with SiO_2-Embedded Elemental Sulfur for Superhydrophobic, Anticorrosion, and Antibacterial Coatings, *ACS Appl. Polym. Mater.*, 2022, **4**(7), 4901–4911.

29 P. Bika, V. Tzitzios, I. Sakellis, S. Orfanoudakis, N. Boukos, S. M. Alhassan, P. Tsipas, V. Psycharis, T. Stergiopoulos and P. Dallas, Electron transfer and energy exchange between a covalent organic framework and $CuFeS_2$ nanoparticles, *J. Mater. Chem. C*, 2024, **12**, 10475–10486.

30 E. Dautzenberg, M. Lam, T. Nikolaeva, W. M. J. Franssen, B. van Lagen, I. P. A. M. Gerrits-Benneheij, N. Kosinov, G. Li and L. C. P. M. de Smet, Tuning UV Absorption in Imine-Linked Covalent Organic Frameworks via Methylation, *J. Phys. Chem. C*, 2022, **126**(50), 21338–21347.

31 H. Li, T. Liang, X. Lai, X. Su, L. Zhang and X. Zeng, Vapor-liquid interfacial reaction to fabricate superhydrophilic and underwater superoleophobic thiol-ene/silica hybrid decorated fabric for oil/water separation, *Appl. Surf. Sci.*, 2018, **427**, 92–101.

32 L. B. Poole, The basics of thiols and cysteines in redox biology and chemistry, *Free Radical Biol. Med.*, 2015, **80**, 148–157.

33 P. Gao, K. Tang, R. Lou, X. Liu, R. Wei, N. Li and B. Tang, Covalent Organic Framework-Based Spherical Nucleic Acid Probe with a Bonding Defect-Amplified Modification Strategy, *Anal. Chem.*, 2021, **93**(35), 12096–12102.

34 Y. Pan, X. Zhang, W. He, L. Zheng and X. Han, Dha Tab-COF filled PEBAX mixed matrix membranes for effective CO_2/CH_4 separation, *Chin. J. Chem. Eng.*, 2025, **77**, 123–134.

35 Z. Kuodis, I. Matulaitienė, M. Špandyreva, L. Labanauskas, S. Stončius, O. Eicher-Lorka, R. Sadzevičienė and G. Niaura, Reflection Absorption Infrared Spectroscopy Characterization of SAM Formation from 8-Mercapto-N-(phenethyl)octanamide Thiols with Phe Ring and Amide Groups, *Molecules*, 2020, **25**(23), 5633.

36 Z. B. Khorshid, M. M. Doroodmand and S. Abdollahi, UV–Vis. spectrophotometric method for oil and grease determination in water, soil and different mediates based on emulsion, *Microchem. J.*, 2021, **60**, 105620.

37 Y. Zhang, G. D. Bland, J. Yan, A. Avellan, J. Xu, Z. Wang, T. P. Hoelen, F. Lopez-Linares, E. S. Hatakeyama, K. Matyjaszewski, R. D. Tilton and G. V. Lowry, Amphiphilic Thiol Polymer Nanogel Removes Environmentally Relevant Mercury Species from Both Produced Water and Hydrocarbons, *Environ. Sci. Technol.*, 2021, **55**, 1231–1241.

38 J. Yan, J. Cao, L. Xue, S. Feng, H. Zhang and D. Wang, Thiol Oxidative Coupling Synthesis of Silicone Foams for Oil/Water Separation, *ACS Appl. Polym. Mater.*, 2020, **2**(4), 1634–1643.

39 F.-C. Wu, R.-L. Tseng and R.-S. Juang, Characteristics of Elovich equation used for the analysis of adsorption

kinetics in dye-chitosan systems, *Chem. Eng. J.*, 2009, **150**, 366–373.

40 A. Kayan, M. O. Arican, Y. Boz, U. Ay and S. K. Bozdas, Novel tyrosine-containing inorganic–organic hybrid adsorbent in removal of heavy metal ions, *J. Environ. Chem. Eng.*, 2014, **2**, 935–942.

41 Z. Yang, S. Fang, M. Duan, Y. Xiong and X. Wang, Chemisorption mechanism of crude oil on soil surface, *J. Hazard. Mater.*, 2020, **386**, 121991.

42 R. Gurav, S. K. Bhatia, T.-R. Choi, Y.-K. Choi, H. J. Kim, H.-S. Song, S. L. Park, H. S. Lee, S. M. Lee, K.-Y. Choi and Y.-H. Yang, Adsorptive removal of crude petroleum oil from water using floating pinewood biochar decorated with coconut oil-derived fatty acids, *Sci. Total Environ*, 2021, **781**, 146636.

43 A. K. Nayak and A. Pal, Development and validation of an adsorption kinetic model at solid-liquid interface using normalized Gudermannian function, *J. Mol. Liq.*, 2019, **276**, 67–77.

44 X. Li, Z. Jia, H.-W. Tan and Y. Yang, Li-An Hou, Enhanced simultaneous adsorption and detection of mercury (II) using functionalized metal – organic framework with defect structures, *Sep. Purif. Technol.*, 2025, **354**(7), 129110.

45 Y. Wang, S. Li, X. Wu, J. Zhang, J. Feng, M. Li, S. Zong and W. Yan, Nitrogen-Based conjugated microporous polymers for efficient Hg(II) removal from Water: Performance and mechanism, *Chem. Eng. J.*, 2023, **471**, 144659.

46 F.-S. Zhang, J. O. Nriagu and H. Itoh, Mercury removal from water using activated carbons derived from organic sewage sludge, *Water Res.*, 2005, **39**(2–3), 389–395.

47 L.-Y. Chai, Q.-W. Wang, Y.-Y. Wang, Q.-Z. Li, Z.-H. Yang and Y.-D. Shu, Thermodynamic study on reaction path of Hg(II) with S(II) in solution, *J. Cent. South Univ. Technol.*, 2010, **17**, 289–294.

48 B. Shi, H. Li, X. Fu, C. Zhao, A. H. Wang, W. Tan, Y. Rao, M. Li, S. Komarneni and H. Yang, Insight into the key role of imine groups in polyaniline for adsorbing heavy metal ions: Density functional theory and experimental study, *Sep. Purif. Technol.*, 2024, **335**, 125866.

49 T. Velempini and K. Pillay, Sulphur functionalized materials for Hg(II) adsorption: A review, *J. Environ. Chem. Eng.*, 2019, **7**(5), 103350.